Performance Analysis of Non-Paraxial Deployments Continuous Aperture MIMO for Electromagnetic Information Theory

Yin Zhang[1,2], Zhouzhuo Guo[1], Bokai Xu[1,2], Jiayi Zhang[1,2], Huahua Xiao[3], Wei E. I. Sha[4], and Bo Ai[1,2]

1. *School of Electronic and Information Engineering, Beijing Jiaotong University, Beijing, 100044, China*
2. *The State Key Laboratory of Advanced Rail Autonomous Operation, Beijing, 100044, China*
3. *ZTE Corporation, The State Key Laboratory of Mobile Network and Mobile Multimedia Technology, Shenzhen, 518055, China*
4. *College of Information Science and Electronic Engineering, Zhejiang University, Hangzhou, 310027, China*

Corresponding author: Jiayi Zhang, Bo Ai; Email: jiayizhang@bjtu.edu.cn, boai@bjtu.edu.cn.

Abstract — Continuous aperture multiple-input multiple-output (CAP-MIMO) has been regarded as the ultimate form of MIMO technology because of its dense antenna elements, offering enhanced system performance. For continuous-spatial electromagnetic channels, the input is continuous current density and the output is continuous electric field. Therefore, it is necessary to obtain the channel characteristics at any point by applying the principles of electromagnetic information theory. In this paper, we provide a closed-form expression for mutual information between continuous transceivers. Then, we expand it to general network deployments beyond the widely studied paraxial setting. Theoretical capacity limits of the communication systems are analyzed to reveal the impact of non-paraxial deployments on the performance of CAP-MIMO systems. The results illustrate that non-paraxial deployments cause more severe fading in signal transmission and different phase offsets for different antenna elements, leading to multipath effects. Moreover, we investigate the impact of key parameters such as azimuth angles, sampling density, and receiver mobility on non-paraxial CAP-MIMO systems.

Keywords — Continuous aperture multiple-input multiple-output (CAP-MIMO), electromagnetic information theory (EIT), mutual information, user mobility, non-paraxial deployment.

I. Introduction

Continuous-Aperture MIMO replaces the conventional array of discrete antennas with a quasi-continuous electromagnetic surface, aiming to exercise fine-grained control over the current distribution across the entire aperture. By directly modulating information onto the shape of spatial electromagnetic waves, CAP-MIMO can generate arbitrary radiation patterns and exploit the physical aperture more efficiently to approach the theoretical capacity limit of finite-sized antennas. Owing to these unique features, CAP-MIMO has emerged as a promising paradigm for sixth-generation (6G) networks [1–4]. Its quasi-continuous aperture architecture [5] enables higher antenna density, spectral efficiency, and spatial degrees of freedom compared with traditional massive MIMO systems [6], thereby improving channel capacity and mutual information and further advancing communication performance [7–10].

The analysis of the CAP-MIMO system with the aid of electromagnetic information theory (EIT) has resulted in numerous research achievements. In [11], the authors have proposed a general EIT analysis framework based on solving eigen-systems of the transceiver. Furthermore, an analytical framework based on EIT to ascertain the performance limits between continuous transceivers was presented in [12], which combined EIT with continuous transceivers and provided a perspective for evaluating the performance of continuous systems. Furthermore, the authors of [13] developed a plane-wave scalar channel model that is applicable in the reactive near-field region. They achieved this by applying physical principles and representing the channel with a correlated random field distributed over the receiving region. The superiority of EIT was demonstrated in [14]. In particular, this paper introduced parameters such as velocity and concentration of power in different directions and raised a concept of the electromagnetic kernel which can capture the tri-polarized nature and smoothly integrate the angular concentrated properties of the electromagnetic fields. [15] focuses on the capacity constrained by generalized angular

Electromagnetic Science

distributions and finite array apertures, highlighting them as critical factors influencing channel capacity.

Among EIT, Green's functions play a significant role. A comprehensive discussion on Green's functions is provided in [16], which explores their applications in wireless communication and electromagnetic compatibility. The authors in [17] analyze MIMO system performance from the electromagnetic degrees of freedom perspective. While existing works have progressed and provided a solid theoretical foundation, the models they discussed often involve paraxial deployments or scenarios where the receiver sizes can be overlooked. In practice, non-paraxial operation commonly arises with large electrical apertures, high carrier frequencies, and short ranges, where spherical wavefronts make paraxial plane-wave models inaccurate, the receivers often have a degree of mobility. In this near-field regime, spherical propagation enables spatial focusing and additional usable spatial degrees of freedom, so mutual information can exceed a paraxial baseline when geometry is properly aligned. Building on this observation, we develop a physics-grounded, computable EIT framework that maps non-paraxial geometry to field correlation and mutual information, pinpointing where non-paraxiality helps, where it hurts and yields actionable deployment guidance. This is a scenario less explored in prior literature. Therefore, analyzing the system performance of CAP-MIMO under non-paraxial deployments is essential.

Motivated by the above observations, this correspondence aims to discuss the mutual information of non-paraxial deployment CAP-MIMO systems. We model the channel using the Green's function based on EIT and describe the electromagnetic field of the channel medium utilizing Maxwell's equations. Meanwhile, we conduct simulations focusing on factors such as the degree of non-paraxiality, azimuth angle, and the number of antennas (discrete points) that could potentially impact channel characteristics. Additionally, we investigate the impact of receiver mobility on system performance.

II. System Model

As shown in Fig. 1, we consider a CAP-MIMO system consisting of the transmitter V_s and the receiver V_r located in two spatial domains. For any arbitrary position $\mathbf{s}$ on the transmitter, its current density can be represented as $\mathbf{J}(\mathbf{s},t) = \Re\{\mathbf{J}(\mathbf{s})\mathrm{e}^{-\mathrm{i}\omega t}\}$, $\mathbf{s} \in \mathbb{R}^3$, and correspondingly, the electric field intensity generated at the receiver $\mathbf{r}$ is denoted as $\mathbf{E}(\mathbf{r},t) = \Re\{\mathbf{E}(\mathbf{r})\mathrm{e}^{-\mathrm{i}\omega t}\}$, $\mathbf{r} \in \mathbb{R}^3$. In time-harmonic form, time t does not affect the expressions of the aforementioned current density and electric field intensity, obtaining $\mathbf{J}(\mathbf{s})$ and $\mathbf{E}(\mathbf{r})$. Based on the Maxwell's equation, the electromagnetic wave equation on a single frequency point is

$$\nabla \times \nabla \times \mathbf{E}(\mathbf{r}) - \kappa_0^2 \mathbf{E}(\mathbf{r}) = \mathrm{i}\kappa_0 Z_0 \mathbf{J}(\mathbf{r}), \tag{1}$$

where $\kappa_0 = \frac{2\pi}{\lambda}$ is the spatial wavenumber. $Z_0 = 120\pi\ \Omega$ is the spatial impedance. ∇ is the differential operator. The dyadic Green's function is defined as

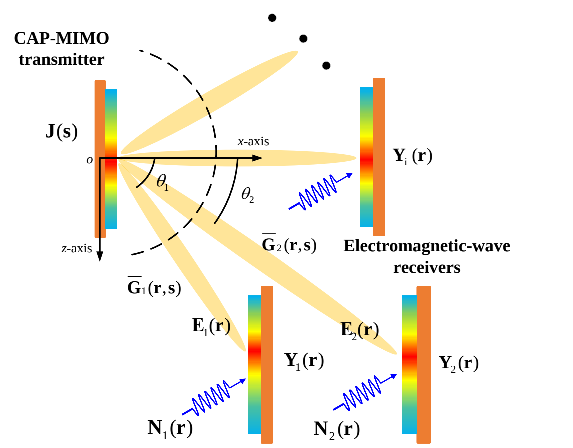

Figure 1 Non-paraxial CAP-MIMO system model. The current density $\mathbf{J}(\mathbf{s})$ on the transmitter aperture generates the received electric field $\mathbf{E}_i(\mathbf{r})$. The azimuth angle θ quantifies the misalignment between the transceivers' axes. The received signal $\mathbf{Y}_i(\mathbf{r})$ includes the desired field $\mathbf{E}_i(\mathbf{r})$ and additive noise $\mathbf{N}_i(\mathbf{r})$.

$$\nabla \times \nabla \times \bar{\mathbf{G}}(\mathbf{r},\mathbf{s}) - \kappa_0^2 \bar{\mathbf{G}}(\mathbf{r},\mathbf{s}) = \bar{\mathbf{I}}\delta(\mathbf{r},\mathbf{s}). \tag{2}$$

According to the Sommerfeld radiation conditions and (2), (1) can be solved as

$$\mathbf{E}(\mathbf{r}) = \int_{V_s} \bar{\mathbf{G}}(\mathbf{r},\mathbf{s}) \cdot \mathbf{J}(\mathbf{s})\mathrm{d}\mathbf{s},\ \mathbf{r} \in V_r. \tag{3}$$

This equation represents the integral form of the wave equation solution using the dyadic Green's function, which serves as the channel model in this work, describing how electromagnetic waves propagate from the source distribution $\mathbf{J}(\mathbf{s})$ in volume V_s to the observation point $\mathbf{r}$ in volume V_r.

In free space, the dyadic Green's function $\bar{\mathbf{G}}(\mathbf{r},\mathbf{s})$ models the vector nature of wave propagation from each point source. It can be expressed as

$$\bar{\mathbf{G}}(\mathbf{r},\mathbf{s}) = (\bar{\mathbf{I}} + \frac{\nabla\nabla}{\kappa_0^2}) g(\|\mathbf{r}-\mathbf{s}\|), \tag{4}$$

where $g(\|\mathbf{r}-\mathbf{s}\|) = \frac{\mathrm{i}\kappa_0 Z_0}{4\pi} \frac{\mathrm{e}^{\mathrm{i}\kappa_0\|\mathbf{r}-\mathbf{s}\|}}{\|\mathbf{r}-\mathbf{s}\|}$ is the scalar Green's function. Moreover, considering the influence of the noise in space, the field observed by the receiver $\mathbf{Y}(\mathbf{r})$ not only includes the information-carrying electric field $\mathbf{E}(\mathbf{r})$ but also incorporates the superposition of the thermal noise field $\mathbf{N}(\mathbf{r})$, which is modeled as

$$\mathbf{Y}(\mathbf{r}) = \mathbf{E}(\mathbf{r}) + \mathbf{N}(\mathbf{r}),\ \mathbf{r} \in V_r. \tag{5}$$

Due to the stochastic nature of the transmitter generating the smallest unit of information, the electromagnetic field before entering the propagation medium is randomly excited by the transmitter. Additionally, for better statistical analysis of the signal, the electromagnetic field is modeled as a Gaussian random field. It should be noted that although the electric field may not be Gaussian in all scenarios, the Gaussian assumption provides a worst-case estimate of mutual information under power constraints, offering a conservative performance estimate for the system. We express the matrix-valued functions of the autocorrelation functions of the transmitter current density and receiver electric field intensity as $\bar{\mathbf{R}}_{\mathbf{J}}(\mathbf{s},\mathbf{s}') = \mathbb{E}[\mathbf{J}(\mathbf{s})\mathbf{J}^{\mathrm{H}}(\mathbf{s}')]$ and $\bar{\mathbf{R}}_{\mathbf{E}}(\mathbf{r},\mathbf{r}') = \mathbb{E}[\mathbf{E}(\mathbf{r})\mathbf{E}^{\mathrm{H}}(\mathbf{r}')]$, respectively. Moreover, we can further express the autocorrelation function of the current density as

$$\bar{\mathbf{R}}_{\mathbf{J}}(\mathbf{s},\mathbf{s}') = \mathbb{E}[\mathbf{J}(\mathbf{s})\mathbf{J}^{\mathrm{H}}(\mathbf{s}')] = \delta(\mathbf{s}-\mathbf{s}')\mathbf{I}\ (A^2/\mathrm{m}^4). \tag{6}$$

It is noteworthy that in practical antenna array deployments, mutual coupling between antenna elements is an inevitable effect. This phenomenon can be mathematically modeled by introducing a linear operator $\mathbf{M}$ on the source current. More formally, in the continuous domain, this operator is represented by an integral kernel $\mathbf{M}(\mathbf{s},\mathbf{s}')$, which characterizes the coupling relationship between the current densities at $\mathbf{s}'$ and $\mathbf{s}$. However, both mutual coupling and non-paraxial deployments degrade system performance. If both effects were considered simultaneously, it would be difficult to disentangle their respective contributions to the performance loss. Therefore, to isolate the impact of non-paraxial deployments and maintain analytical clarity, we set $\mathbf{M}$ to the identity operator $\mathbf{I}$ in this paper. This simplification corresponds to setting its kernel $\mathbf{M}(\mathbf{s},\mathbf{s}')$ to the Dirac delta function $\delta(\mathbf{s}-\mathbf{s}')$, effectively assuming a coupling-free scenario. Consequently, the analysis herein establishes a theoretical performance upper bound.

According to (3), the dyadic Green's function can characterize the relationship between $\bar{\mathbf{R}}_{\mathbf{J}}$ and $\bar{\mathbf{R}}_{\mathbf{E}}$:

$$\begin{aligned}\bar{\mathbf{R}}_{\mathbf{E}}(\mathbf{r},\mathbf{r}') &= \int_0^{L_s}\int_0^{L_s} \bar{\mathbf{G}}(\mathbf{r},\mathbf{s})\cdot\bar{\mathbf{R}}_{\mathbf{J}}(\mathbf{s},\mathbf{s}')\cdot\bar{\mathbf{G}}^{\mathrm{H}}(\mathbf{r}',\mathbf{s}')\mathrm{d}\mathbf{s}\mathrm{d}\mathbf{s}' \\ &= \int_0^{L_s}\bar{\mathbf{G}}(\mathbf{r},\mathbf{s})\cdot\bar{\mathbf{G}}^{\mathrm{H}}(\mathbf{r}',\mathbf{s})\mathrm{d}\mathbf{s}.\end{aligned} \tag{7}$$

Next, we also express the matrix-valued functions of the autocorrelation functions of the electric field observed by the receiver and the noise field considered in the preceding text, denoted as $\bar{\mathbf{R}}_{\mathbf{Y}}(\mathbf{r},\mathbf{r}') = \mathbb{E}[\mathbf{Y}(\mathbf{r})\mathbf{Y}^{\mathrm{H}}(\mathbf{r}')]$ and $\bar{\mathbf{R}}_{\mathbf{N}}(\mathbf{r},\mathbf{r}') = \mathbb{E}[\mathbf{N}(\mathbf{r})\mathbf{N}^{\mathrm{H}}(\mathbf{r}')]$ respectively. Subsequently, leveraging information theory and the closed-form solution of mutual information for finite-length linear transceivers as discussed in [12], we can obtain

$$I(\mathbf{E};\mathbf{Y}) = \log\det\left(\mathbf{I}+\frac{\bar{\mathbf{T}}_{\mathbf{E}}}{n_0/2}\right), \tag{8}$$

where n_0 represents the one-sided power spectral density of Gaussian white noise, and $\bar{\mathbf{T}}_{\mathbf{E}}$ denotes the integration operator associated with the information-bearing electric field. From the autocorrelation functions, we can gain further insights into the integral operator $\bar{\mathbf{T}}_{\mathbf{E}}$:

$$\begin{aligned}\bar{\mathbf{T}}_{\mathbf{E}} &= \mathbb{E}\left[\int_0^{L_r}\mathbf{E}(\mathbf{r})\mathrm{d}\mathbf{r}\int_0^{L_r}\mathbf{E}^*(\mathbf{r}')\mathrm{d}\mathbf{r}'\right] \\ &= \int_0^{L_r}\int_0^{L_r}\bar{\mathbf{R}}_{\mathbf{E}}(\mathbf{r},\mathbf{r}')\mathrm{d}\mathbf{r}\mathrm{d}\mathbf{r}'.\end{aligned} \tag{9}$$

Combining equations (9) and (7) into equation (8), we derive an explicit expression for mutual information between continuous transceivers, computable numerically for non-paraxial deployments, i.e.,

$$I = \log\det\left(\mathbf{I}+\frac{\int_0^{L_r}\int_0^{L_r}\int_0^{L_s}\bar{\mathbf{G}}(\mathbf{r},\mathbf{s})\cdot\bar{\mathbf{G}}^{\mathrm{H}}(\mathbf{r}',\mathbf{s})\mathrm{d}\mathbf{s}\mathrm{d}\mathbf{r}\mathrm{d}\mathbf{r}'}{n_0/2}\right). \tag{10}$$

In complex propagation scenarios, the received field can be modeled as a superposition of N_p components:

$$\mathbf{E}(\mathbf{r}) = \sum_{i=1}^{N_p}\alpha_i\int_{V_s}\overline{\mathbf{G}}_i(\mathbf{r},\mathbf{s})\cdot\mathbf{J}(\mathbf{s})\,\mathrm{d}\mathbf{s} + \mathbf{N}(\mathbf{r}), \tag{11}$$

where $\alpha_i \sim \mathcal{CN}(0,\sigma_i^2)$. The corresponding field correlation and mutual information read

$$\overline{\mathbf{R}}_E(\mathbf{r},\mathbf{r}') = \sum_{i=1}^{N_p}\sigma_i^2\int_{V_s}\overline{\mathbf{G}}_i(\mathbf{r},\mathbf{s})\cdot\overline{\mathbf{G}}_i^{\mathrm{H}}(\mathbf{r}',\mathbf{s})\,\mathrm{d}\mathbf{s}, \tag{12}$$

$$I_{\mathrm{NLoS}} = \log\det\left(\mathbf{I}+\frac{\sum_{i=1}^{N_p}\sigma_i^2\,\bar{\mathbf{T}}_{\mathbf{E},\mathbf{i}}}{n_0/2}\right). \tag{13}$$

In practice, per-path excess attenuation due to partial blockage can be absorbed as $\sigma_i^2 \leftarrow L_i\,\sigma_i^2$ with $0 < L_i \leq 1$, which preserves the mutual-information form in (10) while enabling scenario-specific calibration from measurements or standardized models.

Then, we further describe the dyadic Green's function. For the complete matrix representation of the dyadic Green's function (4), its specific expansion yields

$$\overline{\mathbf{G}} = \begin{bmatrix} G_{xx} & G_{xy} & G_{xz} \\ G_{yx} & G_{yy} & G_{yz} \\ G_{zx} & G_{zy} & G_{zz}\end{bmatrix}. \tag{14}$$

Each element in the Green's function matrix represents the interaction between specific directional polarization components, reflecting the response of electromagnetic waves in different polarization directions. Here, we adopt a different method involving linear arrays as discussed in [12]. When parallel misalignment occurs in linear array configurations, the approximation method of considering only the G_{zz} elements of the Green's function matrix along the z-direction field may not always be applicable. For rigor in our discussion, we also considered tri-polarization.

Electromagnetic Science

Although this paper focuses on continuous aperture configurations, the methodological framework in this study is fundamentally applicable to arbitrary aperture geometries. This generality stems from the theory's foundation in Maxwell's equations in integral form.

III. Performance Analysis of CAP-MIMO Systems

In this section, we evaluate the performance of the system in general network deployments based on the system model and relevant formulas established in the previous section.

• *Impact of azimuth angles and transceiver positions on the mutual information:* In actual network deployments, V_s and V_r are not necessarily parallel to each other. Thus, non-paraxial deployments are considered. As shown in Fig. 1, we define the azimuth angle, which influences the channel function between transceivers and thus leads to variations in channel gains. The central points of V_s and V_r are denoted as $\mathbf{c}_s = (x_{sc}, y_{sc}, z_{sc})$ and $\mathbf{c}_r = (x_{rc}, y_{rc}, z_{rc})$. The distance between the transceivers is $R = \|\mathbf{r} - \mathbf{s}\| = \sqrt{\sum_a (a_{rc} - a_{sc})^2},\ \ a \in \{x, y, z\}$. V_s and V_r are not necessarily parallel to one another, and an arbitrary angle (the azimuth angle θ) with respect to the $x\text{-}axis$, and an arbitrary angle (the azimuth angle φ) with respect to the $y\text{-}axis$. θ and φ have equal status. Therefore, to simplify the discussion, we will only consider the linear array model in case $\varphi = 0$ as follows. At the same time, to ensure that mutual visibility between surfaces is appropriately taken into account in our analysis, the azimuth angle $\theta \in (\frac{\pi}{2}, \frac{\pi}{2})$.

The received electric field is primarily obtained through calculations based on the transmitter's current density and channel function. When the current density is fixed, the received electric field can be considered to be influenced solely by the channel function. Therefore, we can get the system performance by analyzing the channel function (4).

The equation (4) expresses the dyadic Green's function in the form of the scalar Green's function $g(\|\mathbf{r} - \mathbf{s}\|)$ multiplied by a dyadic vector. We perform similar operations on $\mathbf{J}(\mathbf{s})$ and $\mathbf{E}(\mathbf{r})$, transforming them into scalar multiplied by a vector. $\mathbf{J}_k(\mathbf{s}) = J_k(\mathbf{s}) \cdot \mathbf{u}_k$, $\mathbf{E}_j(\mathbf{r}) = E_j(\mathbf{r}) \cdot \mathbf{u}_j$, where k and j denote k-th component of $\mathbf{J}(\mathbf{s})$ and j-th component of $\mathbf{E}(\mathbf{r})$. Thus, the equation (3) can be rewritten as

$$\mathbf{E}_j(\mathbf{r}) = \int_{V_s} (\bar{\mathbf{I}} + \frac{\nabla\nabla}{\kappa_0^2}) g(\|\mathbf{r}_j - \mathbf{s}_k\|) \cdot \mathbf{u}_j \cdot \mathbf{u}_k \cdot J_k(\mathbf{s}) \mathrm{d}\mathbf{s}, \quad (15)$$

where $\mathbf{r}_k = (x_{rc}, y_{rc}, z_{rc} + \Delta z_r)$, $\mathbf{s}_k = (x_{sc}, y_{sc}, z_{sc} + \Delta z_s)$. Δz is the distance from the component to the center point. The dyadic vector $\left[(\bar{\mathbf{I}} + \frac{\nabla\nabla}{\kappa_0^2}) \cdot \mathbf{u}_j\right] \cdot \mathbf{u}_k$ accounts for the coupling between the j-th component of the surface current density $\mathbf{J}(\mathbf{s})$ and the k-th component of the received electric field $\mathbf{E}(\mathbf{r})$. The scalar Green's function $g(\|\mathbf{r}_j - \mathbf{s}_k\|)$ accounts for the fading characteristics of the channel.

Considering the azimuth angle θ, the fading factor $\|\mathbf{r}_j - \mathbf{s}_k\|$ of the only variable in the scalar Green's function can be rewritten as

$$\begin{aligned} \|\mathbf{r}'_j - \mathbf{s}_k\| &= \sqrt{(Rcos\theta)^2 + (\Delta z_r + Rsin\theta)^2} \\ &= \sqrt{R^2 + 2\Delta z_r Rsin\theta + (\Delta z_r)^2} \\ &\overset{(\alpha)}{>} \|\mathbf{r}_j - \mathbf{s}_k\| \sqrt{1 + \frac{2\Delta z_r sin\theta}{\|\mathbf{r}_j - \mathbf{s}_k\|}} \\ &\overset{(\beta)}{\approx} \|\mathbf{r}_j - \mathbf{s}_k\| + \Delta z_r sin\theta. \end{aligned} \quad (16)$$

It is worth mentioning that to facilitate theoretical analysis, (α) reduces the fading factor, and the actual fading caused by non-paraxial will be more severe. (β) follows from the parabolic approximation $\sqrt{1+t} \approx 1 + t/2$ and can be applied in the near field if the transceiver sizes are not too large compared to the distance R. Based on (16), the scalar Green's function can be rewritten as

$$g(\|\mathbf{r}' - \mathbf{s}\|) = \frac{\mathrm{i}\kappa_0 Z_0}{4\pi} \frac{\mathrm{e}^{\mathrm{i}\kappa_0\|\mathbf{r}-\mathbf{s}\|} \cdot \mathrm{e}^{\mathrm{i}\kappa_0 \Delta z_r sin\theta}}{\|\mathbf{r} - \mathbf{s}\| + \Delta z_r sin\theta}. \quad (17)$$

According to (17), it can be observed that from the amplitude perspective, the channel fading becomes more severe due to the influence of non-paraxial deployments, and from the phase perspective, non-paraxial deployments cause different phase shifts across antennas, leading to multipath effects.

• *Impact of azimuth angles on the channel function:* We use a Fourier transform on the channel function under the corresponding conditions to investigate how azimuth angle affects channel characteristics. Therefore, the spatial spectral density at the receiver can be expressed by

$$\bar{\mathbf{S}}_{\mathbf{E}}(\kappa) = 2\pi \bar{\mathbf{S}}_{\mathbf{J}}(\kappa) \cdot \left|\bar{\mathbf{G}}(\kappa)\right|^2, \quad (18)$$

where $\left|\bar{\mathbf{G}}(\kappa)\right|$ is the Fourier transform of the channel function and $\bar{\mathbf{S}}_{\mathbf{J}}(\kappa)$ represents the spatial spectral density at the transmitter. This equation reveals the relationship between the transmitter current density in the spatial domain, the receiver electric field intensity, and the channel function. When $\bar{\mathbf{G}}(\kappa)$ is relatively large, it indicates that it can provide a more prominent channel gain at the corresponding wavenumber, thereby reflecting the channel function characteristics.

• *Impact of receiver mobility on the channel function:* We introduce the receiver's velocity to explore its influence on the channel. Specifically, due to the relative motion between the receiving antenna and the transmission medium, the received signal exhibits a frequency offset, commonly referred to as the Doppler effect[16]. We assume the receiver moves away from the transmitter at the velocity v. When a plane wavefront arrives at the receiver, the distance to the next wavefront at the receiver is λ. Since the receiver is moving away from the transmitter, the time it takes for the receiver to receive the next wavefront is

$$t = \frac{\lambda}{c - v} = \frac{c}{f_s(c - v)}, \quad (19)$$

Electromagnetic Science

where f_s is the frequency corresponding to the speed of light c. Taking into account the time dilation effect of relativity, the time observed by the receiver is $t' = t/\gamma$, where the Lorentz factor is

$$\gamma = \frac{1}{\sqrt{1 - v^2/c^2}}. \tag{20}$$

Therefore, the frequency observed by the receiver is given by

$$f' = \frac{1}{t'} = \frac{\gamma f_s (c - v)}{c}. \tag{21}$$

Based on the frequency-shift property of the Fourier transform, the receiver's velocity causes a spectrum shift. This is also a reflection of the Doppler effect.

The EIT model extends directly to three-dimensional, time-varying motion. Let the receiver velocity be $\mathbf{v}(t)$ and $\phi(\mathbf{r}, t)$ the instantaneous phase of the incident wave. The instantaneous Doppler shift is

$$\Delta f_d(\mathbf{r}, t) = \frac{1}{\lambda}\, \mathbf{v}(t) \cdot \nabla_{\mathbf{r}} \phi(\mathbf{r}, t), \tag{22}$$

which, for a plane wave with $\mathbf{k} = \kappa_0 \hat{\mathbf{n}}$, reduces to

$$\Delta f_d(t) = \frac{\kappa_0}{2\pi}\, \mathbf{v}(t) \cdot \hat{\mathbf{n}}. \tag{23}$$

The Doppler-induced phase is absorbed into the field of (3) as

$$\mathbf{E}(\mathbf{r}, t) = \int_{V_s} \overline{\mathbf{G}}(\mathbf{r}, \mathbf{s}) \cdot \mathbf{J}(\mathbf{s})\, d\mathbf{s} \cdot \mathrm{e}^{-\mathrm{i}2\pi \int_0^t \Delta f_d(\tau) \mathrm{d}\tau}, \tag{24}$$

so that the correlation operator and the mutual-information expressions in (7) - (10) follow with $\mathbf{E}(\mathbf{r}, t)$ in place of $\mathbf{E}(\mathbf{r})$. We next illustrate the 1D constant-velocity case in (19) - (21) for clarity.

IV. Simulation Results

In this section, the transceivers are placed in parallel along the z-axis on the xz-plane. In order to comprehensively cover the near-field and far-field regions, the wavelength λ is set to 1 m, but the conclusion can be extended to the typical high-frequency of CAP-MIMO systems. The length of the transceiver panel is set to 2λ and the power density of noise is 1 ($\mathrm{V}^2/\mathrm{m}^2$)*.

• *Impact of the azimuth angle and the distance on the system performance:* To examine the effect of azimuth angle on system performance, we set the distance between transceivers at 3 m, 5 m, and 10 m. Then, we vary the azimuth angle of the system θ from $-\frac{\pi}{2}$ to $\frac{\pi}{2}$ with a step size of $\frac{\pi}{10}$. It can be observed from Fig. 2 that the mutual information of the system is symmetric about $\theta = 0$. As the azimuth angle $|\theta|$ increases, the mutual information of the system decreases correspondingly. Additionally, the system's mutual information decreases as the Euclidean distance increases. The smaller the azimuth angle $|\theta|$, the greater the impact of the Euclidean distance on the mutual information. As $|\theta|$ approaches $\frac{\pi}{2}$, the mutual information values of the system under different Euclidean distances tend to converge.

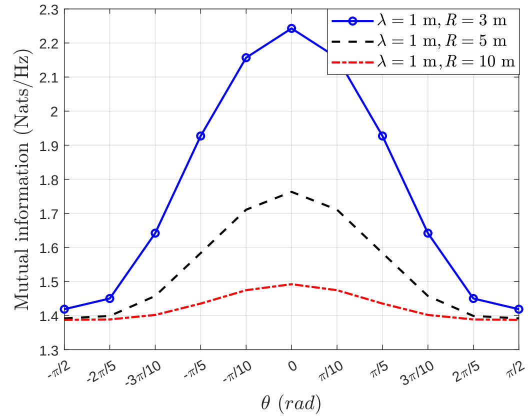

Figure 2 Mutual information with different distances between transceivers R and azimuth angles θ.

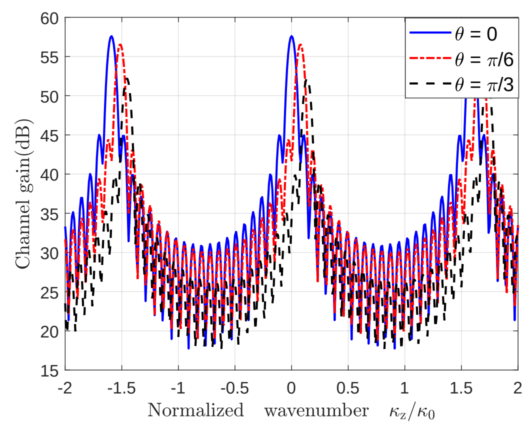

Figure 3 Fourier transform of the channel function with different azimuth angles θ and normalized wavenumber κ_z/κ_0.

In Fig. 3, to investigate further the influence of azimuth angles, we set the Euclidean distance between the transmitter and receiver to 5 m and consider azimuth angles of 0, $\frac{\pi}{6}$ and $\frac{\pi}{3}$. It is obvious that in the wavenumber domain, the main lobe gain of the channel decreases with the increase of θ. Additionally, there is an observable phenomenon of deviation in the wavenumber domain.

Fig. 4 reveals the impact of azimuth angles and Euclidean distances on mutual information. We vary non-paraxial degree $Rsin\theta$ from 0 to 4 m in increments of 0.2 m. The receiver is moved along the x-axis from 1m to 15 m in increments of 0.5 m. We can observe that under the same horizontal distance x between transceivers, the mutual information of the

*The unit $\mathrm{V}^2/\mathrm{m}^2$ for the noise power density is a direct consequence of modeling noise as a physical random electric field, whose unit is V/m. The variance of this field, which represents its power, therefore has the unit of $(\mathrm{V/m})^2 = \mathrm{V}^2/\mathrm{m}^2$.

Electromagnetic Science

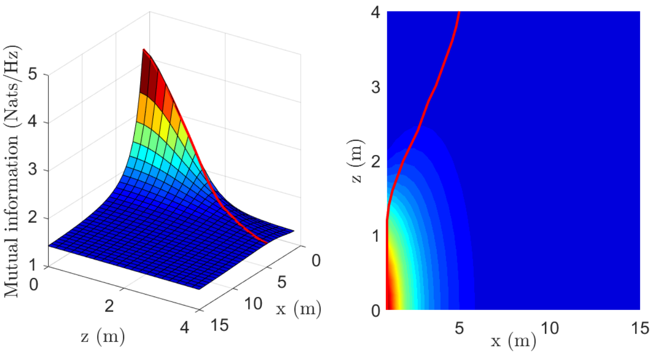

Figure 4 Impact of non-paraxial degree on mutual information. The left figure shows the 3D surface plot, while the right figure presents the corresponding heatmap. The red curve on the heatmap traces the maximum mutual information.

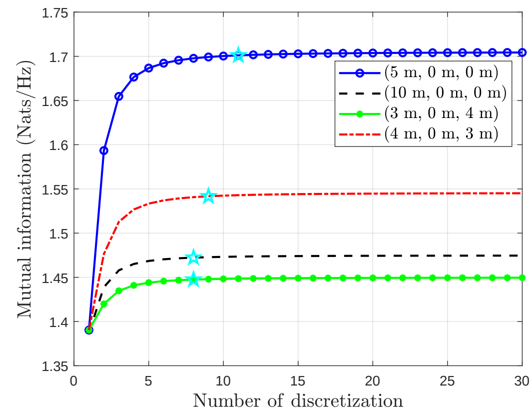

Figure 5 The x-axis represents the number of discretization points, and the y-axis is the mutual information measured at different positions. With increasing discretization points, the mutual information gradually converges to the continuous-space value.

system decreases with an increase in the non-paraxial degree. Additionally, fixing the non-paraxial degree and varying the horizontal distance x, the mutual information exhibits a trend of initially increasing and then decreasing with the increase of x. It means that there exists at a point x where the system's mutual information reaches its maximum value. The red line represents the line connecting the x value corresponding to the maximum mutual information.

• *Impact of the positions and discrete point numbers on the mutual information:* In Fig. 5, we change the number of discrete points (the number of antennas) from 1 to 30 and set the position of the transmitter at (0 m, 0 m, 0 m) and the receiver at (5 m, 0 m, 0 m), (10 m, 0 m, 0 m), (3 m, 0 m, 4 m) and (4 m, 0 m, 3 m), respectively. All curves exhibit a convergence phenomenon as the number of discrete points increases. Blindly increasing sampling points does not infinitely improve system performance. The optimal number depends on multiple factors, including the Euclidean distance between the transceivers, the degree of non-paraxial deployment, the signal wavelength, the transceiver size, and the channel conditions.

• *Impact of velocity changes on the channel gain:* We previously conducted a theoretical analysis of how mobile receivers affect the system's channel characteristics in the frequency domain. In this subsection, we simulate the Doppler phenomenon resulting from the theoretical analysis. Similar to [12], we focus on the field along the z-direction. To obtain the performance of Fourier transforms on the channel functions, we vary the receiver velocities to 100 m/s, 500 m/s, and 800 m/s, and the results are shown in Fig. 6. We can observe that the Doppler effect is induced by the receiver's velocity. Although it is not prominently evident due to its relatively small magnitude, we can observe it from specific data. Additionally, as the receiver velocity increases, the channel gain decreases accordingly due to reduced frequency.

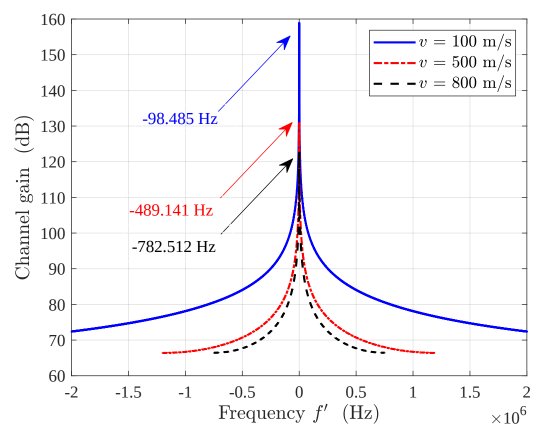

Figure 6 Impact of Doppler effect on system performance. Channel gain over the frequency observed by the receiver with different velocities.

V. Conclusion

In this paper, we discussed the system's mutual information and spectral characteristics under non-paraxial deployments. We revealed the influence of non-paraxial deployments and sampling numbers on mutual information and examined the impact of receivers' velocity on channel gain. Through simulations, we demonstrated that non-paraxial deployments reduce mutual information and channel gain. Moreover, when the degree of non-paraxial deployments is fixed, the mutual information of the system exhibits a trend of initially increasing and then decreasing with the receiver's movement. Finally, we validated the Doppler effect in the CAP-MIMO system. Further work can explore mitigation techniques like adaptive beamforming with dynamic current density optimization, multi-scale receiver sampling, and edge computing-assisted RIS to address fading and phase offsets in non-paraxial CAP-MIMO systems, while incorporating practical constraints. Further optimization of algorithms to determine optimal azimuths, sampling points, and receiver configurations for deployment is also critical.

References

[1] H. Tataria, M. Shafi, A. F. Molisch, M. Dohler, and H. Sjöland, "6G wireless systems: Vision, requirements, challenges, insights, and opportunities", *Proc. IEEE*, vol.109, no.7, pp.1166–1199, 2021.

[2] J. Zhang, E. Björnson, M. Matthaiou, D. W. K. Ng, *et al.*, "Prospective multiple antenna technologies for beyond 5G", *IEEE J. Sel. Areas Commun.*, vol.38, no.8, pp.1637–1660, 2020.

[3] Z. Wang, J. Zhang, H. Du, D. Niyato, *et al.*, "A tutorial on extremely large-scale MIMO for 6G: Fundamentals, signal processing, and applications", *IEEE Commun. Surveys Tuts.*, vol.26, no.3, pp.1560–1605, 2024.

[4] Z. Liu, J. Zhang, Z. Liu, H. Du, *et al.*, "Cell-free XL-MIMO meets multi-agent reinforcement learning: Architectures, challenges, and future directions", *IEEE Wirel. Commun.*, vol.31, no.4, pp.155–162, 2024.

[5] C. Huang, S. Hu, G. C. Alexandropoulos, A. Zappone, *et al.*, "Holographic MIMO surfaces for 6G wireless networks: Opportunities, challenges, and trends", *IEEE Wirel. Commun.*, vol.27, no.5, pp.118–125, 2020.

[6] B. Xu, J. Zhang, Z. Chen, B. Cheng, *et al.*, "Channel estimation for rydberg atomic receivers", *IEEE Wirel. Commun. Lett.*, in press, pp.1–1, 2025.

[7] S. Chen, J. Zhang, E. Björnson, J. Zhang, and B. Ai, "Structured massive access for scalable cell-free massive MIMO systems", *IEEE J. Sel. Areas Commun.*, vol.39, no.4, pp.1086–1100, 2021.

[8] E. Björnson, C.-B. Chae, R. W. H. Jr, T. L. Marzetta, *et al.*, "Towards 6G MIMO: Massive spatial multiplexing, dense arrays, and interplay between electromagnetics and processing", *arXiv:2401.02844*, in press, 2024.

[9] B. Xu, J. Zhang, H. Du, Z. Wang, *et al.*, "Resource allocation for near-field communications: Fundamentals, tools, and outlooks", *IEEE Wirel. Commun.*, vol.31, no.5, pp.42–50, 2024.

[10] A. Poon, R. Brodersen, and D. Tse, "Degrees of freedom in multiple-antenna channels: A signal space approach", *IEEE Trans. Inf. Theory*, vol.51, no.2, pp.523–536, 2005.

[11] F. K. Gruber and E. A. Marengo, "New aspects of electromagnetic information theory for wireless and antenna systems", *IEEE Trans. Antennas Propag.*, vol.56, no.11, pp.3470–3484, 2008.

[12] Z. Wan, J. Zhu, Z. Zhang, L. Dai, and C.-B. Chae, "Mutual information for electromagnetic information theory based on random fields", *IEEE Trans. Commun.*, vol.71, no.4, pp.1982–1996, 2023.

[13] A. Pizzo, L. Sanguinetti, and T. L. Marzetta, "Spatial characterization of electromagnetic random channels", *IEEE Open J. Commun. Soc.*, vol.3, pp.847–866, 2022.

[14] J. Zhu, Z. Wan, L. Dai, and T. Cui, "Can electromagnetic information theory improve wireless systems? A channel estimation example", *arXiv:2310.12446*, in press, 2023.

[15] J. Z. Y. Zhang, Y. Zhang, Y. Yao, and G. Liu, "Capacity analysis of holographic MIMO channels with practical constraints", *IEEE Wirel. Commun. Lett.*, vol.12, no.6, pp.1101–1105, 2023.

[16] W. E. I. Sha, L. Ying, and G. Xiao, "Green's functions in electromagnetism", *Physics*, vol.53, no.1, pp.43–49, 2024.

[17] S. S. A. Yuan, Z. He, X. Chen, C. Huang, and W. E. I. Sha, "Electromagnetic effective degree of freedom of an MIMO system in free space", *IEEE Antennas Wireless Propag. Lett.*, vol.21, no.3, pp.446–450, 2022.

Yin Zhang received the B.S. degree in communication engineering from Beijing Jiaotong University, China, in 2025, where he is currently pursuing the M.S. degree. His research interests include eelectromagnetic information theory, quantum wireless communication, and optimization theory of wireless systems. (Email: 25120225@bjtu.edu.cn)

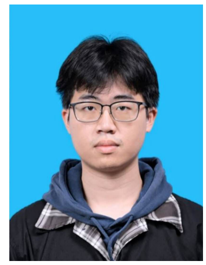

Zhouzhuo Guo received the B.S. degree in communication engineering from Beijing Jiaotong University, China, in 2025. In the summer of 2025, he was a Visiting Student at Duke University ECE, USA. His research interests include machine learning and electromagnetic information theory. (Email: 21231273@bjtu.edu.cn)

Bokai Xu received the B.S. degree in communication engineering from Beijing Jiaotong University, China, in 2024, where he is currently pursuing the Ph.D. degree. He has been a Visiting Student with the School of Electrical & Electronic Engineering, The University of Hong Kong, Hong Kong, since November 2024. His research interests include machine learning, signal processing, and optimization theory of wireless systems. (Email: 20251197@bjtu.edu.cn)

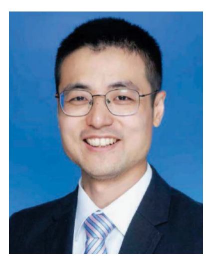

Jiayi Zhang (Senior Member, IEEE) received the B.Sc. and Ph.D. degrees in communication engineering from Beijing Jiaotong University, China, in 2007 and 2014, respectively.
Since 2016, he has been a Professor with the School of Electronic and Information Engineering, Beijing Jiaotong University. From 2014 to 2016, he was a Post-Doctoral Research Associate with the Department of Electronic Engineering, Tsinghua University, China. From 2014 to 2015, he was also a Humboldt Research Fellow of the Institute for Digital Communications, Friedrich-Alexander-University Erlangen-Nürnberg (FAU), Germany. His current research interests include cell-free massive MIMO, reconfigurable intelligent surface, XL-MIMO, near-field communications, and applied mathematics. He received the Best Paper Awards at the IEEE ICC 2023, WCSP 2017 and 2024, and IEEE APCC 2017; the URSI Young Scientist Award in 2020; and the IEEE ComSoc Asia–Pacific Outstanding Young Researcher Award in 2020. He was a Lead Guest Editor of the Special Issue on "Multiple Antenna Technologies for Beyond 5G" of the IEEE Journal on Selected Areas in Communications, a Lead Guest Editor of the Special Issue on "Semantic Communications for the Metaverse" of IEEE Wireless Communications, an Editor of IEEE Communications Letters from 2016 to 2021, and an Editor of IEEE Transactions on Communications from 2019 to 2024. He also serves as an Associate Editor for IEEE Transactions on Wireless Communications. (Email: zhangjiayi@bjtu.edu.cn)

Huahua Xiao received the M.S. degree in computer software and theories from Sun Yat-sen University, Guangzhou, China. He is currently a Senior Engineer in antenna algorithm pre-research with ZTE Corporation, Shenzhen, China. He has applied for more than 150 Chinese and foreign patents in the multi-antenna field. (Email: xiao.huahua@zte.com.cn)

Wei E. I. Sha Wei E. I. Sha (Senior Member, IEEE) received the B.S. and Ph.D. degrees in electronic engineering from Anhui University, Hefei, China, in 2003 and 2008, respectively.,From July 2008 to July 2017, he was a Post-Doctoral Research Fellow and later a Research Assistant Professor with the Department of Electrical and Electronic Engineering, The University of Hong Kong. In October 2017, he joined the College of Information Science and Electronic Engineering, Zhejiang University, Hangzhou, China, where he is currently a tenured Associate Professor. From March 2018 to March 2019, he held the Marie Skłodowska-Curie Individual Fellowship with University College London. He has authored or co-authored over 200 peer-reviewed journal articles, 180 conference papers, 12 book chapters, and two books. His work has been cited over 11,700 times on Google Scholar, with an H-index of 58. His research interests include theoretical and computational electromagnetics, such as computational and applied electromagnetics, nonlinear and quantum electromagnetics, micro- and nano-optics, and multiphysics modeling.,Dr. Sha is a Life Member of OSA. He received multiple awards, including the ACES-China Electromagnetics Education Ambassador Award in 2024, the ACES Technical Achievement Award in 2022, and the PIERS Young Scientist Award in 2021. Nine of his students have won best student paper awards. He is an Associate Editor of IEEE Journal on Multiscale and Multiphysics Computational Techniques, IEEE Open Journal of Antennas and Propagation, IEEE Access, and Electromagnetic Science. He has reviewed more than 60 technical journals and served on the Technical Program Committees of over ten IEEE conferences. (Email: weisha@zju.edu.cn)

Bo Ai (Fellow, IEEE) received the master's and Ph.D. degrees from Xidian University, China, and the Graduate degree from Tsinghua University.
He received the honor of Excellent Post-Doctoral Research Fellow with Tsinghua University in 2007. He was a Visiting Professor with the EE Department, Stanford University, in 2015. He is currently with Beijing Jiaotong University as a Full Professor and a Ph.D. Candidate Advisor. He is also the Deputy Director of the State Key Laboratory of Rail Traffic Control and Safety and the Deputy Director of the International Joint Research Center. He is one of the main responsible people for Beijing "Urban rail operation control system" International Science and Technology Cooperation Base and the Backbone Member of the Innovative Engineering Base jointly granted by Chinese Ministry of Education and the State Administration of Foreign Experts Affairs. He has authored/co-authored eight books and published over 300 academic research articles in his research area. He has 26 invention patents. He has been the research team leader for 26 national projects and has won some important scientific research prizes. Five articles have been the ESI highly-cited articles. He has been notified by Council of Canadian Academies (CCA) that, based on Scopus database, he has been listed as one of the top 1% authors in his field all over the world. He has also been feature interviewed by *IET Electronics Letters*. His research interests include the research and applications of channel measurement and channel modeling and dedicated mobile communications for rail traffic systems.

Prof. Ai is a Fellow of the Institution of Engineering and Technology (IET Fellow) and the IEEE VTS Distinguished Lecturer. He is an IEEE VTS Beijing Chapter Vice Chair and the IEEE BTS Xi'an Chapter Chair. He was also a co-chair or a session/track chair of many international conferences. He is an Editor of IEEE Antennas and Wireless Propagation Letters and IEEE Transactions on Consumer Electronics and was an Editorial Committee Member of *Wireless Personal Communications*. He is a Lead Guest Editor of Special Issues on IEEE Transactions on Vehicular Technology, IEEE Antennas and Propagation Letters, and the *International Journal on Antennas and Propagation*. He has received many awards, such as the Distinguished Youth Foundation and Excellent Youth Foundation from the National Natural Science Foundation of China, the New Century Excellent Talent Award by Hong Kong Qiushi Foundation, the New Century Talents by the Chinese Ministry of Education, and the Zhan Tianyou Railway Science and Technology Award by the Beijing Municipality Science and Technology Commission. (Email: boai@bjtu.edu.cn)